Microwave-assisted rapid synthesis of Sb_2Te_3 nanosheets and thermoelectric properties of bulk samples prepared by spark plasma sintering

Guo-Hui Dong, Ying-Jie Zhu* and Li-Dong Chen

Received 24th July 2009, Accepted 23rd November 2009
First published as an Advance Article on the web 21st January 2010
DOI: 10.1039/b915107a

Sb_2Te_3 single-crystalline nanosheets having edge lengths of 300–500 nm and thicknesses of 50–70 nm were rapidly synthesized by a microwave-assisted method using $SbCl_3$, Na_2TeO_3 and hydrazine hydrate in ethylene glycol at 200 °C for 15 min, and the reaction mechanism was proposed. The bulk sample of Sb_2Te_3 nanosheets was prepared by spark plasma sintering (SPS), and it still consisted of Sb_2Te_3 nanosheets after SPS and thermoelectric property measurements. High electrical conductivity σ ($2.49 \times 10^4\ \Omega^{-1}\ m^{-1}$), high Seebeck coefficient S ($210\ \mu V\ K^{-1}$) and low thermal conductivity κ ($0.76\ W\ m^{-1}\ K^{-1}$) at 420 K were achieved. The ZT value was reported for the first time for the Sb_2Te_3 sintered bulk sample prepared from nanosheet powder, and a relatively high ZT of 0.58 at 420 K was obtained. It is very difficult to achieve high electrical conductivity σ without obvious growth of nanocrystals after sintering, and herein we have made a successful attempt.

Introduction

Thermoelectric (TE) materials, which can convert waste heat to useful electrical energy for power generation and lower the temperature for refrigeration due to the Seebeck and Peltier effects, respectively, are expected to play an increasingly important role in solving the energy crisis in the future. The wide applications of TE materials have been restrained by the low energy conversion efficiency, which is represented by the dimensionless figure-of-merit $ZT = S^2\sigma T/\kappa$, where S is the Seebeck coefficient, σ is the electrical conductivity, $S^2\sigma$ is the power factor, k is the thermal conductivity, and T is the absolute temperature.[1] So, how to significantly enhance ZT is a crucial factor for wide applications of TE materials. Reducing the dimensionality and size of the building blocks of TE materials is an efficient and promising way to improve ZT, which has been demonstrated by both theoretical calculations and experimental investigations.[2–11] For example, one-dimensional (1-D) quantum rods or 2-D quantum wells of Bi_2Te_3 with a diameter or well width of 5 Å may attain $ZT = 14$ or 5 by theoretical calculations;[5] and ZT values of 2.4, 1.47 and 1.4 have been attained from Bi_2Te_3/Sb_2Te_3 nanolayer superlattice films at room temperature,[4] Bi_2Te_3/Sb_2Te_3 bulk nanocomposites at 450 K[8] and nanostructured bismuth antimony telluride bulk alloys at 373 K,[10] respectively.

Antimony telluride (Sb_2Te_3) has attracted great attention for high σ ($(3.13–5.26) \times 10^5\ \Omega^{-1}\ m^{-1}$ at 300 K) and low k (1.6–5.6 W $m^{-1}\ K^{-1}$ at 300 K) of the single crystal.[12] Unfortunately, the S of the undoped Sb_2Te_3 single crystal is too low (83–92 $\mu V\ K^{-1}$ at 300 K)[12] to obtain high ZT although it has high σ and low k. However, higher S can be attained by introducing nanostructures, for example, 125 $\mu V\ K^{-1}$ at room temperature was reported for a film of Sb_2Te_3 nanoplates[13] and 185 $\mu V\ K^{-1}$ at 505 K for a thin film grown by co-evaporation.[14] Unfortunately, the measured σ values of both films were only $10^2\ \Omega^{-1}\ m^{-1}$, which were far lower than that of the undoped Sb_2Te_3 single crystal. It is very difficult to attain high σ for nanomaterials, and the advantages of nanomaterials are easily obscured by their low σ, although very high ZT values of nanomaterials have been predicted by theoretical calculations.

Many methods have been developed to synthesize antimony telluride nanostructures with different morphologies, such as vapor–liquid–solid (VLS) for growing nanowires,[15] aerosol-assisted chemical vapor deposition for nanofilms,[16] chemical vapor deposition by decomposition of metallorganic precursor for nanoplates[17] and nano-lamellae,[18] mechanical alloying for preparing nanocrystallites,[19] electrochemical deposition using a porous alumina template,[20] electrochemical atomic layer epitaxy for preparing nanofilms,[21] hydro-/solvo-thermal treatment for preparing nanorods,[22] nanobelts,[23] anisotropic nanocrystals,[24] nanoforks[25] and nanoplates,[13,26–28] and microwave heating for preparing nanoplates.[29] Unfortunately, in many previous methods, long reaction times were needed, and the products usually contained elemental tellurium (Te) as an impurity. Te is a semimetal and contains free electrons, so Te may neutralize the positive holes of the p-type semiconductor Sb_2Te_3 and lead to a significant decrease in σ and $S^2\sigma$,[30] and low σ is one of the key problems for TE nanomaterials.

Herein, we report a microwave-assisted solvothermal method for the rapid synthesis of hexagonal Sb_2Te_3 single-crystalline nanosheets. The microwave-assisted solvothermal method is attracting increasing attention for the advantages such as rapid heating and high reaction rate which reduces the preparation time often by orders of magnitude, leading to very high efficiency and energy saving.[31,32] To the best of our knowledge, ZT values have not been reported for Sb_2Te_3 sintered bulk samples compacted from nanosheet powders. Up to now, few successful

State Key Laboratory of High Performance Ceramics and Superfine Microstructure, Shanghai Institute of Ceramics, Chinese Academy of Sciences, Shanghai, 200050, P. R. China. E-mail: y.j.zhu@mail.sic.ac.cn; Fax: +86-21-52413122; Tel: +86-21-52412616

investigations have been reported on sintered bulk TE materials with high ZT prepared from nanopowders without significant growth of nanocrystals. In this paper, we have made a successful attempt and report for the first time the ZT values of the Sb_2Te_3 nanosheet bulk samples sintered by spark plasma sintering (SPS), and Sb_2Te_3 nanosheets were well preserved after SPS and TE property measurements. Relatively good TE properties have been achieved in the Sb_2Te_3 nanosheet sintered bulk sample from 300 K to 420 K: high σ ($(2.33–2.49) \times 10^4\ \Omega^{-1}\ m^{-1}$), high S (147–210 $\mu V\ K^{-1}$) and low κ (1.02–0.76 $W\ m^{-1}\ K^{-1}$), and $ZT = 0.58$ at 420 K.

Experimental

Synthesis of Sb_2Te_3 nanosheet powders

All chemicals were purchased and used without further purification. In a typical synthetic procedure: $SbCl_3$ (0.137 g) and Na_2TeO_3 (0.200 g) were dissolved in ethylene glycol (EG, 26 mL) under vigorous stirring to form a colorless clear solution, then it was added into a 60 mL Teflon autoclave, followed by the addition of hydrazine hydrate ($N_2H_4 \cdot H_2O$, 85% (wt.%), 6.5 mL). The solution quickly became dark in a few seconds and the dark suspension was stirred vigorously for about 1 min, and then the Teflon autoclave was sealed and microwave-heated rapidly to 200 °C and maintained at this temperature for 15 min, and then cooled down naturally. The precipitate was collected by centrifugation, and ultrasonically washed with deionized water two times and ethanol once, and dried at 60 °C in vacuum. The microwave oven used for sample preparation was a microwave solvothermal synthesis system (MDS-6, Sineo, Shanghai, China), and the experimental parameters such as the temperature, heating rate and reaction time can be well controlled.

Preparation of Sb_2Te_3 nanosheet sintered bulk samples

A typical sintering procedure was as follows: the nanosheet powder (about 1.2 g) without precompaction was sintered by spark plasma sintering (SPS) at 270 °C under a pressure of 67 MPa for about 6 min in a graphite die in vacuum (about 6 Pa) and then cooled naturally to room temperature. The sintered sample was a circular tablet with a diameter of 10 mm and thickness of about 2.7 mm, which was cut into a cuboid with sizes of $2.7 \times 4 \times 9$ mm.

Characterization of samples

The products were characterized by X-ray powder diffraction (XRD) (Rigaku Dmax 2550V X-ray diffractometer with Cu-Kα radiation ($\lambda = 1.54178$ Å)). The morphology and size of the samples were investigated by field-emission scanning electron microscopy (SEM) (JEOL JSM-6700F), energy dispersive spectroscopy (EDS, Gensis 2000), field-emission transmission electron microscopy (TEM) and selected area electron diffraction (SAED) (JEOL JEM-2100F). The thermogravimetry (TG) and differential scanning calorimetry (DSC) were measured with a TG-DTA/DSC thermal analyzer (Netzsch, Germany) with a heating rate of 10 °C min^{-1} in flowing nitrogen gas.

Thermoelectric property measurements

The electrical conductivity σ was measured by the standard four-probe method in vacuum. The Seebeck coefficient S was obtained from the slope of the thermoelectromotive force (ΔE) *versus* the temperature difference (ΔT) plot in vacuum. The thermal conductivity $k = \rho D C_p$ was calculated from the measured thermal diffusivity D, specific heat C_p, and density ρ. D was measured by a laser flash method (Shinkuriko, TC-7000) in vacuum; C_p was measured in a differential scanning calorimetry apparatus (Perkin Elmer, DSC-2C) in flowing nitrogen. Density ρ was measured with the Archimedes principle. The dimensionless figure of merit ZT was calculated by using the values of S, σ and κ at the given temperature.

Results and discussion

The XRD pattern of the Sb_2Te_3 powder prepared by the microwave solvothermal method is shown in Fig. 1a. The diffraction peaks can be well indexed to a single phase of well-crystallized Sb_2Te_3 with a hexagonal structure (JCPDS, No. 15-0874). No impurities such as elemental Te are detected by XRD, showing that this method is rapid and efficient for the preparation of single-phase Sb_2Te_3 without the formation of elemental Te. In the previous reports,[23,25,28] elemental Te was formed as an impurity together with Sb_2Te_3. The impurity Te can significantly decrease carrier concentration, which gives rise to low σ and low $S^2\sigma$. Our experiments show that the formation of Te has something to do with the ratio of Na_2TeO_3 to $SbCl_3$. Te formed in the presence of excess Na_2TeO_3 even when the reaction

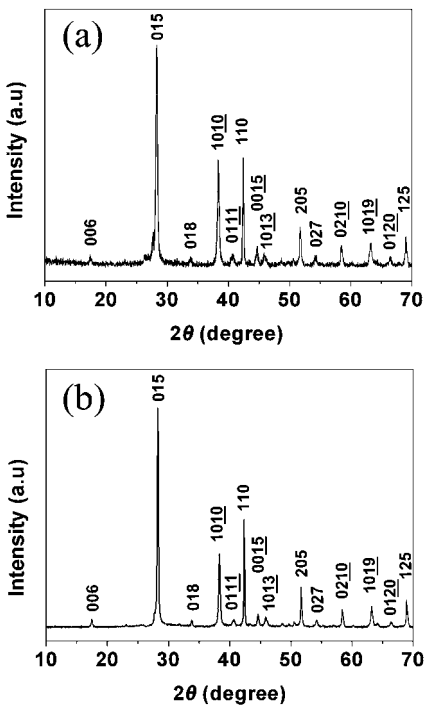

Fig. 1 XRD patterns. (a) The Sb_2Te_3 powder prepared by the microwave solvothermal method using $SbCl_3$, Na_2TeO_3 and hydrazine hydrate in ethylene glycol at 200 °C for 15 min; (b) the Sb_2Te_3 nanosheet bulk sample sintered by SPS in vacuum at 270 °C for 6 min.

time was prolonged to 60 min. The XRD pattern of the Sb_2Te_3 nanosheet sintered bulk sample prepared by SPS is shown in Fig. 1b, which indicates that the chemical composition of the sintered bulk sample was still a single phase of Sb_2Te_3.

To further clarify the reaction mechanism involved in the formation of Sb_2Te_3, a series of comparison experiments were performed. $SbCl_3$ was dissolved in EG and excess hydrazine hydrate without addition of Na_2TeO_3, followed by microwave heating to 200 °C and kept at this temperature for 20 min, and no precipitate formed, indicating no formation of elemental Sb. In contrast, when Na_2TeO_3 was dissolved in EG without addition of $SbCl_3$, a dark blue suspension appeared slowly when excess hydrazine hydrate was added at room temperature, indicating that TeO_3^{2-} was reduced to Te or even Te^{2-}. The question is whether dismutation reaction of Te occurs in the alkaline environment as shown in eqn (1)[13,29,33] or Te is reduced by hydrazine hydrate as in eqn (2)?

$$3Te + 6OH^- = TeO_3^{2-} + 2Te^{2-} + 3H_2O \quad (1)$$

$$2Te + N_2H_4 + 4OH^- = 2Te^{2-} + N_2 + 4H_2O \quad (2)$$

According to the cell potentials:

$$E^{\theta}(TeO_3^{2-}/Te) = -0.57\ V;\ E^{\theta}(Te/Te^{2-}) = -0.84\ V;$$
$$E^{\theta}(N_2/N_2H_4) = -1.15\ V$$

the potentials of the cells may be calculated as follows:

$$E^{\theta}_{(1)} = E^{\theta}\left(Te/Te^{2-}\right) - E^{\theta}\left(TeO_3^{2-}/Te\right) = -0.27\ V < 0,$$

$$E^{\theta}_{(2)} = E^{\theta}\left(Te/Te^{2-}\right) - E^{\theta}(N_2/N_2H_4) = 0.31\ V > 0,$$

$$E_{(1)} = E^{\theta}_{(1)} - \frac{RT}{4F}\ln\frac{\left[Te^{2-}\right]^2\left[TeO_3^{2-}\right]}{\left[OH^-\right]^6}$$
$$= -0.27 - \frac{RT\ \ln 10}{4F}\left\{\log\left(\frac{1}{2}\left[Te^{2-}\right]^3\right) + 6\ (14 - pH)\right\}$$

It is known that the cell reaction takes place spontaneously only when the potential of the cell is greater than zero volt ($E > 0$ V). It is obvious that Te is easier to be reduced by hydrazine hydrate, while dismutation reaction of Te only occurs when the concentration of OH^- is very high. The required concentration of OH^- may be approximately calculated as follows:

If $E_{(1)} > 0$,

$$pH > 14 + \frac{1}{6}\left\{\frac{5443}{T} + \log\left(\frac{1}{2}[Te^{2-}]^3\right)\right\}$$

If the concentration of Te^{2-} ($[Te^{2-}]$) is higher than 10^{-4} M and absolute temperature T is lower than 500 K, the calculated pH is larger than 13.76, and the corresponding concentration of OH^- is 0.58 M, this is unlikely to be achieved by hydrazine hydrate itself or other weak alkali. To verify the calculation result, different amounts of NaOH were added into the colorless transparent solution consisting of $SbCl_3$, Na_2TeO_3 and EG without addition of hydrazine hydrate to form 0.5 M or 0.6 M NaOH solutions: elemental Te or a mixture of Te and Sb_2Te_3 were attained, respectively, supporting the above conclusion. In order to confirm that Te can be reduced to Te^{2-} by hydrazine hydrate, highly pure (99.999%) Te powder was added into hydrazine hydrate at room temperature, and a purple characteristic color of Te^{2-} appeared slowly under vigorous stirring at room temperature. Therefore, the reaction mechanism in the present reaction system is that Te is reduced by hydrazine hydrate instead of the dismutation reaction of Te. Herein, we put forward and demonstrate the above-mentioned reaction mechanism for the first time, and the reactants reduced directly were TeO_3^{2-} and Te but not $Sb_2(TeO_3)_3$ because no precipitate appeared when Na_2TeO_3 and $SbCl_3$ were dissolved in EG.

So, the reaction process in the present system may be expressed as follows:

$$TeO_3^{2-} + N_2H_4 = Te + N_2 + H_2O + 2OH^- \quad (3)$$

$$2Te + N_2H_4 + 4OH^- = 2Te^{2-} + N_2 + 4H_2O \quad (4)$$

$$2Sb^{3+} + 3Te^{2-} = Sb_2Te_3 \quad (5)$$

Based on the above reaction mechanism, it is easy to understand why no Sb_2Te_3 one-dimensional nanostructures formed because Te was reduced to Te^{2-} and thus no Te acted as a template. Previous reports proposed that Te played a role of template to generate telluride in the reactions between elemental Te and other elemental reactants, for example, Bi_2Te_3,[34,35] PbTe,[36–38] CdTe,[37] CoTe,[39,40] NiTe[40] and Ag_2Te.[41] However, the reaction mechanism proposed herein is totally different from the previous reports.[34–41]

The morphology and size of the Sb_2Te_3 product were characterized by TEM and SEM, as shown in Fig. 2. Fig. 2 shows that the Sb_2Te_3 product consists of hexagonal nanosheets with edge lengths of 300–500 nm and thicknesses of 50–70 nm. The SAED pattern taken from a single nanosheet reveals that the nanosheet is a well-crystallized single crystal, and the diffraction spots can be assigned to Sb_2Te_3 with a hexagonal structure (Fig. 2c). EDS (Fig. 2f) confirms that the chemical composition of the nanosheet was composed of Sb and Te elements, which is consistent with the XRD result (Fig. 1a).

The TG and DSC curves measured in flowing nitrogen gas showed that the melting point of Sb_2Te_3 nanosheets was 417.9 °C, which is much lower than that of bulk Sb_2Te_3 crystals (620 °C).[42] Sb_2Te_3 nanosheet bulk samples were prepared by SPS at a given temperature below the melting point of Sb_2Te_3 nanosheets.

The temperature dependences of σ, S, $S^2\sigma$, κ and ZT of the Sb_2Te_3 nanosheet bulk sample sintered by SPS are plotted in Fig. 3. The σ values are (2.33–2.49) $\times 10^4\ \Omega^{-1}m^{-1}$ from 200 to 420 K, which are remarkably higher by two orders of magnitude than that of Sb_2Te_3 nanoplate film[13] and Sb_2Te_3 thin film grown by co-evaporation.[14] The biggest bottleneck of TE nanomaterials is the low σ which is mainly dominated by contact resistances between nanoparticles.[43] In the Sb_2Te_3 nanosheet sintered bulk sample, the high σ may be attributed to relative high density and sheet-like morphology, which are favorable for sufficient contacts among nanosheets. Sufficient contacts may decrease the excessive scattering of electrons and lead to a reduction in contact resistance. The relative density of the Sb_2Te_3 nanosheet sintered bulk sample was about 89%.

The S values are 147–216 $\mu V\ K^{-1}$ from 300 K to 480 K. The S at room temperature is 147 $\mu V\ K^{-1}$, which is much higher than

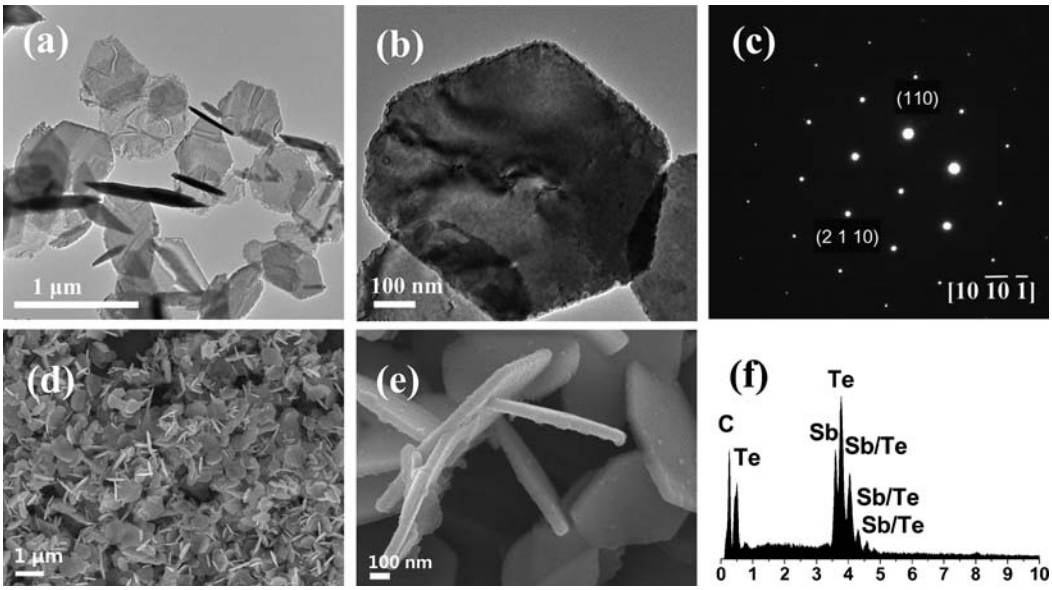

Fig. 2 TEM and SEM micrographs and EDS of Sb_2Te_3 nanosheets prepared by the microwave solvothermal method using $SbCl_3$, Na_2TeO_3 and hydrazine hydrate in ethylene glycol at 200 °C for 15 min. (a,b) TEM micrographs; (c) SAED pattern taken from a single nanosheet; (d) low-magnification SEM micrograph; (e) high-magnification SEM micrograph; (f) EDS.

that of undoped Sb_2Te_3 single crystal (83 μV K^{-1} along the cleavage planes and 92 μV K^{-1} in the perpendicular direction at 300 K)[12] and Sb_2Te_3 nanoplate film (125 μV K^{-1} at room temperature).[13] S has reached 210 μV K^{-1} at 420 K, which is larger than that of an Sb_2Te_3 thin film grown by co-evaporation (185 μV K^{-1} at 505 K).[14] In the temperature range of measurement, the highest S is 216 μV K^{-1} at 480 K. The high S may result from quantum confinement effects and size effects in Sb_2Te_3 nanosheets, which may help to adjust electron and phonon transport and change the energy band structure, energy level and electronic density of states, leading to the improvement of the Seebeck coefficient.[2,43]

Low k values (1.02–0.76 W m^{-1} K^{-1} from 300 to 420 K) have been successfully achieved in the Sb_2Te_3 nanosheet sintered bulk sample, and they are lower than that of undoped Sb_2Te_3 single crystals (5.6 W m^{-1} K^{-1} along the cleavage planes and 1.6 W m^{-1} K^{-1} in the perpendicular direction at 300 K),[12] polycrystalline bulk (4.7 W m^{-1} K^{-1} at 300 K)[44] and the bulk consisting of nanoparticles compacted by hot pressing (about 2.0–1.6 W m^{-1} K^{-1} from 300 K to 450 K).[24] The strong phonon scattering by a large quantity of crystal interfaces in the Sb_2Te_3 nanosheet sintered bulk sample may contribute to low k. It should be noted that the crystal interfaces in the Sb_2Te_3 nanosheet sintered bulk sample not only scatter phonons but also scatter electrons strongly, resulting in low σ.[43] It is well known that the mean free paths of electrons are usually longer than those of phonons for a semiconductor at a given temperature above room temperature. So, an effective strategy to greatly improve σ without k rising significantly is to improve the density of the sample to shorten the distances among the nanostructures without removing crystal interfaces. The ideal distance among the nanoparticles should be shorter than the mean free path of electrons but longer than that of phonons; in this way, only phonons can be strongly scattered without obvious electron scattering. The calculated $S^2\sigma$ values of the Sb_2Te_3 nanosheet sintered bulk sample are 0.51–1.06 mW m^{-1} K^{-2} from 300 K to 420 K.

The dimensionless figure-of-merit ZT values of the Sb_2Te_3 nanosheet sintered bulk sample are 0.15 at 300 K and 0.58 at

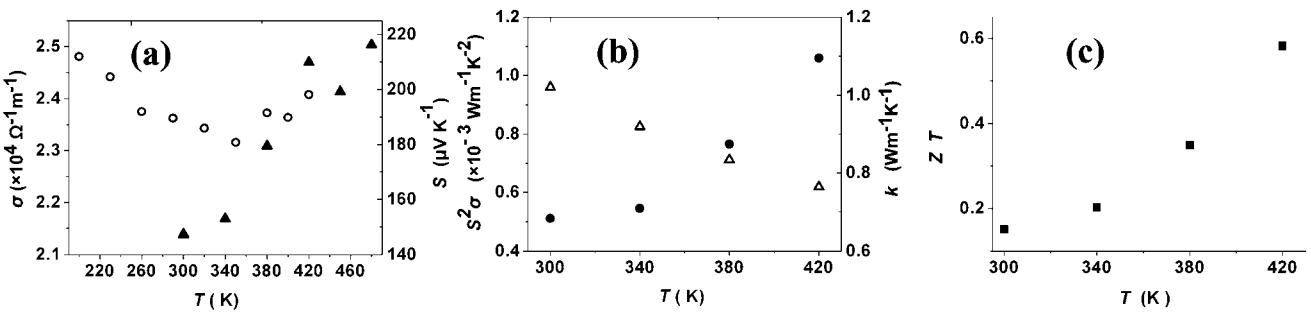

Fig. 3 The temperature (T) dependences of thermoelectric properties of the Sb_2Te_3 nanosheet bulk sample sintered by SPS: (a) electrical conductivity σ (○) and Seebeck coefficient S (▲); (b) power factor $S^2\sigma$ (●) and thermal conductivity κ (△); (c) the dimensionless figure-of-merit ZT (■).

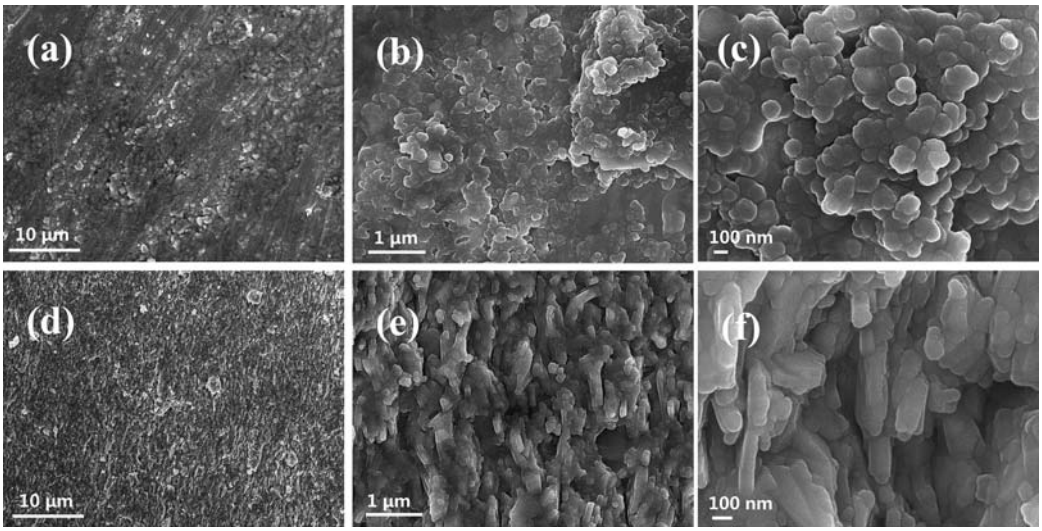

Fig. 4 SEM micrographs of Sb_2Te_3 nanosheet bulk samples after measurements of all thermoelectric properties. (a–c) Surface plane of the samples, and (d–f) cross-section of the samples.

420 K, and the estimated ZT at 480 K is higher than 0.70. The maximum ZT achieved in the Sb_2Te_3 nanosheet sintered bulk sample is higher than that reported for undoped Sb_2Te_3 single crystals. It is reported that the maximum ZT of undoped Sb_2Te_3 single crystals was 0.48 at 300 K,[12] implying that the undoped Sb_2Te_3 single crystals are only suitable for refrigeration but unsuitable for power generation. Compared with the undoped Sb_2Te_3 single crystals, the maximum ZT temperature of the Sb_2Te_3 nanosheet sintered bulk sample moves obviously towards high temperature, which is desirable for application in power generation. The higher ZT of the Sb_2Te_3 nanosheet sintered bulk sample mainly results from higher S and lower k, this is obviously different from that of conventional bulk Sb_2Te_3. Most kinds of conventional bulk TE materials have high σ but high k or low S. The σ of the Sb_2Te_3 nanosheet sintered bulk sample is lower than that of undoped Sb_2Te_3 single crystals ($10^5\ \Omega^{-1}\ m^{-1}$) by one order of magnitude, which means that there is huge potential room for improvement of σ and ZT if higher density of the sample can be attained by suitable molding processes, such as higher molding pressure.

SEM micrographs of the Sb_2Te_3 nanosheet sintered bulk sample after the measurements of TE properties are shown in Fig. 4. It is easy to understand that nanosheets will adopt a preferential orientation under the effect of the applied external high pressure during the SPS process. This is revealed by Fig. 4, which shows both the horizontal surface (a–c) and cross-section (d–f) of the Sb_2Te_3 nanosheet sintered bulk samples. One can see that it is obviously different in the horizontal surface from the cross-section of the sample. The nanosheets lie down parallel to the horizontal surface direction and perpendicular to the cross-section direction. The thicknesses of the nanosheets are about 60–100 nm, indicating the increase in nanosheet thickness compared with those of the powders (50–70 nm) before the SPS process. The sintered bulk sample still consists of Sb_2Te_3 nanosheets after measurements of the TE properties. This verifies the presence of large numbers of nanosheets and crystal interfaces in the Sb_2Te_3 nanosheet sintered bulk sample, accounting for higher S and lower k. Till now, few successful investigations have been reported on bulk TE materials with high ZT prepared from nanostructured powders without significant growth of nanocrystals, and herein, we have made a successful attempt.

Conclusions

Sb_2Te_3 single-crystalline nanosheets have been rapidly synthesized using $SbCl_3$, Na_2TeO_3 and hydrazine hydrate in ethylene glycol at 200 °C for 15 min by a microwave-assisted solvothermal method. The reaction mechanism has been proposed for the formation of Sb_2Te_3 nanosheets. The Sb_2Te_3 nanosheet bulk sample sintered by SPS still consists of nanosheets without significant crystal growth. Higher electrical conductivity σ, higher Seebeck coefficient S and lower thermal conductivity κ have been achieved in the Sb_2Te_3 nanosheet sintered bulk sample. It is very difficult to achieve high electrical conductivity σ without obvious growth of nanocrystals after sintering, and herein, we have made a successful attempt. ZT of 0.58 at 420 K has been obtained and the maximum ZT temperature moves significantly to the high temperature zone, indicating that the Sb_2Te_3 nanosheet sintered bulk materials have potential applications in power generation.

Acknowledgements

This work is supported by the National Natural Science Foundation of China (50821004, 50772124), the Program of Shanghai Subject Chief Scientist (07XD14031) and the Fund for Nano-Science and Technology from Science and Technology Commission of Shanghai (0852nm05800).

Notes and references

1 H. J. Goldsmid, *Thermoelectric Refrigeration*, Plenum Press, New York, 1964.
2 M. S. Dresselhaus, G. Chen, M. Y. Tang, R. G. Yang, H. Lee, D. Z. Wang, Z. F. Ren, J. P. Fleurial and P. Gogna, *Adv. Mater.*, 2007, **19**, 1043–1053.
3 Y. Q. Cao, T. J. Zhu, X. B. Zhao, X. B. Zhang and J. P. Tu, *Appl. Phys. A: Mater. Sci. Process.*, 2008, **92**, 321–324.

4 R. Venkatasubramanian, E. Silvola, T. Colpitts and B. O. Quinn, *Nature*, 2001, **413**, 597–602.
5 L. D. Hicks and M. S. Dresselhaus, *Phys. Rev. B: Condens. Matter*, 1993, **47**, 16631–16634.
6 K. F. Hsu, S. Loo, F. Guo, W. Chen, J. S. Dyck, C. Uher, T. Hogan, E. K. Polychroniadis and M. G. Kanatzidis, *Science*, 2004, **303**, 818–821.
7 T. C. Harman, M. P. Walsh, B. E. Laforge and G. W. Turner, *J. Electron. Mater.*, 2005, **34**, L19–L22.
8 Y. Q. Cao, X. B. Zhao, T. J. Zhu, X. B. Zhang and J. P. Tu, *Appl. Phys. Lett.*, 2008, **92**, 143106.
9 T. C. Harman, P. J. Taylor, M. P. Walsh and B. E. LaForge, *Science*, 2002, **297**, 2229–2232.
10 B. Poudel, Q. Hao, Y. Ma, Y. C. Lan, A. Minnich, B. Yu, X. Yan, D. Z. Wang, A. Muto, D. Vashaee, X. Y. Chen, J. M. Liu, M. S. Dresselhaus, G. Chen and Z. F. Ren, *Science*, 2008, **320**, 634–638.
11 M. Zhou, J. F. Li and T. Kita, *J. Am. Chem. Soc.*, 2008, **130**, 4527–4532.
12 D. M. Rowe, *Thermoelectrics Handbook: Macro to Nano*, CRC Press, New York, 2006, Section III, (Chapter 27), p 16.
13 W. D. Shi, L. Zhou, S. Y. Song, J. H. Yang and H. J. Zhang, *Adv. Mater.*, 2008, **20**, 1892–1897.
14 H. L. Zou, D. M. Rowe and G. Min, *J. Vac. Sci. Technol., A*, 2001, **19**, 899–903.
15 J. S. Lee, S. Brittman, D. Yu and H. Park, *J. Am. Chem. Soc.*, 2008, **130**, 6252–6258.
16 J. S. Ritch, T. Chivers, M. Afzaal and P. O'Brien, *Chem. Soc. Rev.*, 2007, **36**, 1622–1631.
17 S. S. Garje, D. J. Eisler, J. S. Ritch, M. Afzaal, P. O'Brien and T. Chivers, *J. Am. Chem. Soc.*, 2006, **128**, 3120–3121.
18 T. Ikeda, L. A. Collins, V. A. Ravi, F. S. Gascoin, S. M. Haile and G. J. Snyder, *Chem. Mater.*, 2007, **19**, 763–767.
19 M. Zakeri, M. Allahkarami, G. Kavei, A. Khanmohammadian and M. R. Rahimipour, *J. Mater. Sci.*, 2008, **43**, 1638–1643.
20 M. Y. Kim, K. W. Park and T. S. Oh, in *13th International Conference on II–VI Compounds*, Jeju City, South Korea, Sep 10–14, 2007, pp 266–270.
21 J. Y. Yang, W. Zhu, X. H. Gao, S. Q. Bao, X. Fan, X. K. Duan and J. Hou, *J. Phys. Chem. B*, 2006, **110**, 4599–4604.
22 Q. Wang, C. L. Jiang, C. F. Yu and Q. W. Chen, *J. Nanopart. Res.*, 2007, **9**, 269–274.
23 W. D. Shi, J. B. Yu, H. S. Wang and H. J. Zhang, *J. Am. Chem. Soc.*, 2006, **128**, 16490–16491.
24 Z. W. Wang, X. Yan, B. Poudel, Y. Ma, Q. Hao, J. Yang, G. Chen and Z. F. Ren, *J. Nanosci. Nanotechnol.*, 2008, **8**, 452–456.
25 S. Shi, M. Cao and C. Hu, *Cryst. Growth Des.*, 2009, **9**, 2057–2060.
26 G. Q. Zhang, W. Wang, X. L. Lu and X. G. Li, *Cryst. Growth Des.*, 2009, **9**, 145–150.
27 Q. L. Yuan, Q. L. Nie and D. X. Huo, *Curr. Appl. Phys.*, 2009, **9**, 224–226.
28 W. Z. Wang, B. Poudel, J. Yang, D. Z. Wang and Z. F. Ren, *J. Am. Chem. Soc.*, 2005, **127**, 13792–13793.
29 B. Zhou, Y. Ji, Y. F. Yang, X. H. Li and J. H. Zhu, *Cryst. Growth Des.*, 2008, **8**, 4394–4397.
30 A. G. Cullis and P. A. Midgley, *Microscopy of Semiconducting Materials* 2003, Royal Microscopical Society, Great Britain, pp 601–606.
31 Y. J. Zhu, W. W. Wang, R. J. Qi and X. L. Hu, *Angew. Chem., Int. Ed.*, 2004, **43**, 1410–1414.
32 M. Tsuji, M. Hashimoto, Y. Nishizawa, M. Kubokawa and T. Tsuji, *Chem.–Eur. J.*, 2005, **11**, 440–452.
33 F. Cao, W. D. Shi, L. J. Zhao, S. Y. Song, J. H. Yang, Y. Q. Lei and H. J. Zhang, *J. Phys. Chem. C*, 2008, **112**, 17095–17101.
34 Z. L. Chai, Z. P. Peng, C. Wang and H. J. Zhang, *Mater. Chem. Phys.*, 2009, **113**, 664–669.
35 B. Zhou, Y. Zhao, L. Pu and J. J. Zhu, *Mater. Chem. Phys.*, 2006, **96**, 192–196.
36 G. A. Tai, W. L. Guo and Z. H. Zhang, *Cryst. Growth Des.*, 2008, **8**, 2906–2911.
37 H. W. Liang, S. Liu, Q. S. Wu and S. H. Yu, *Inorg. Chem.*, 2009, **48**, 4927–4933.
38 G. A. Tai, B. Zhou and W. L. Guo, *J. Phys. Chem. C*, 2008, **112**, 11314–11318.
39 H. Fan, Y. G. Zhang, M. F. Zhang, X. Y. Wang and Y. T. Qian, *Cryst. Growth Des.*, 2008, **8**, 2838–2841.
40 Q. Peng, Y. J. Dong and Y. D. Li, *Inorg. Chem.*, 2003, **42**, 2174–2175.
41 P. F. Zuo, S. Y. Zhang, B. K. Jin, Y. P. Tian and J. X. Yang, *J. Phys. Chem. C*, 2008, **112**, 14825–14829.
42 J. G. Speight, in *Lange's Handbook of Chemistry*; 16th ed., McGraw-Hill, New York, 2005, Section 1, p 22.
43 A. Bulusu and D. G. Walker, *Superlattices Microstruct.*, 2008, **44**, 1–36.
44 Y. S. Touloukian and D. P. DeWitt, *Thermal Conductivity: Metallic Elements and Alloys*, IFI/Plenum, New York, 1970.